J Ther Eng, Vol. 8, No. 4, pp. 515–528, July 2022

Journal of Thermal Engineering
Web page info: https://jten.yildiz.edu.tr
DOI: 10.18186/thermal.1149694

Journal of Thermal Engineering

Research Article

A critical re-examination of Reynolds analogy for micro-convective flow

Rajan KUMAR[1]*

[1]*Department of Mechanical Engineering, Dr B R Ambedkar National Institute of Technology Jalandhar, Punjab-144011, India*

ARTICLE INFO

Article history
Received: 17 October 2020
Accepted: 12 March 2021

Keywords:
Micro-Convection; Thermophysical Fluid Properties; Heat Transfer; Friction Factor; Non-Dimensionalization

ABSTRACT

The present research numerically investigates the validity of the Reynolds analogy for micro-convective water flow between Stanton number (St) and Fanning friction factor (f_f), taking into account combined fluid properties variations such as temperature-dependent density, viscosity, and thermal conductivity. The Reynolds analogy is suggested to be valid when St increases for thermophysical fluid properties (TFP) with a decrease in f_f. This analogy, therefore, helps to find the flow regime that increases heat transfer while shear stress decreases for TFP. Hence, the Reynolds analogy for TFP helps to design and improve the performance of the different devices, including micro-scale heat exchangers for electronics cooling, internal cooling passages of turbine airfoils, and many biomedical devices. Three modified non-dimensional parameters ($\Pi_{S\rho T}$, $\Pi_{S\mu T}$, and Π_{SkT}) appear from the non-dimensionalization of the governing conservation equations. Using dimensional analysis, the dependence of the friction factor on these parameters is examined.

Cite this article as: Kumar R. A critical re-examination of reynolds analogy for micro-convective flow. J Ther Eng 2022;8(4):515-528.

INTRODUCTION AND REVIEW

The temperature gradients along and across the flow in micro-convective flows are much steeper due to high heat fluxes and low Reynolds number (Re). Consequently, the effects of TFP variations in micro-convective flows can not be neglected. In many industrial applications, heat transfer (HT) from a wall to a flowing fluid stream is an essential process and HT rates affect the performance of the overall system. Therefore, precious attempts were made to raise HT rates and reduce shear stress (τ) to improve system efficiency. Reynolds analogy helps to discover the flow regime in which HT improves while τ drops for TFP. Reynolds analogy for TFP helps to design and optimize the performance of different devices, including micro-scale heat exchangers, micro-scale passages for electronics cooling, internal cooling passages of turbine airfoils, external surfaces of gas turbine airfoils, and many biomedical devices.

Firstly, Sieder and Tate [1] studied the impact of variation in $\mu(T)$ on forced convection (FC). The method of property ratio was used to find $\mu(T)$ variation effect. An asymptotic theory was used to examine the influence of

*Corresponding author.
*E-mail address:

This paper was recommended for publication in revised form by Regional Editor Dr. Chandramohan VP

Published by Yıldız Technical University Press, İstanbul, Turkey

TFP on the fully developed flow (FDF) [2, 3]. The effects of $\mu(T)$ variation on Nusselt number (Nu) and friction factor (f) for laminar flow through a circular tube were analyzed by Kakac et al. [4]. Harms et al. [5] studied laminar FDF in a semicircular duct with $\mu(T)$ variations. It was observed that the $\mu(T)$ variations create significant distortions in both the velocity and temperature distributions.

The influences of TFP on the local temperature, heat flux, and Nu were numerically analyzed [6]. The curvature effect and the effect of variation in $\mu(T)$ on laminar FC and FDF were analyzed [7]. The dependence of Nu and f on $\mu(T)$ variation was analyzed under both cooling and heating conditions. Pure continuum-based micro-convective gas flow with $\rho(T)$ variation was numerically simulated [8]. The physical special effects induced due to $\mu(T)$ and $k(T)$ variations were investigated for the case of laminar micro-convective water flow [9, 10]. The physical effects induced due to variable gas properties in micro-convective flow were reported [11]. The effects of $\mu(T)$ variation can not be overlooked for a wide range of operating conditions in the entry region of straight ducts [12]. Herwig and Mahulikar [13] examined the effects of TFP on single-phase incompressible micro-convective flow. Mahulikar et al. [14] suggested the need to examine the impacts of fluid variation on f. The fluid friction characteristics in laminar FDF were studied and the Reynolds analogy was reexamined for TFP [15]. The effects of TFP on thermally developing flow were numerically studied by Liu et al. [16], in the cooling passages of micro-channel. The effects of fluid variation on single-phase micro-convective compressible flow were investigated [17]. The physical mechanisms induced due to TFP in laminar micro-convective FDF were examined [18]. Because of TFP, a significant difference in pressure drop from macro to micro scale was measured. Gulhane and Mahulikar [19] studied the hydrodynamic and thermally developing flow problem and the Graetz problem due to fluid properties variations. Harley et al. [20] provided theoretical and experimental research on compressible gas flow in micro-channels with a large subsonic Mach number. Kumar and Mahulikar [21] explored the effects of $\mu(T)$ variation on laminar micro-convective FDF. The abnormal HT and fluid flow observations were recognized owing to variability in $\mu(T)$ and these observations were clarified using the concept of thermal and hydrodynamic undevelopment of flow. Frictional flow characteristics of micro-convective flow for TFP were investigated [22]. Recently, Kumar and Mahulikar [23] numerically re-examined the validity of the Chilton-Colburn analogy between $St{\cdot}Pr^{2/3}$ and f_f for laminar micro-convective flow with $\mu(T)$ and $k(T)$ variations. Kumar and Mahulikar [24] numerically investigated the heat transfer characteristics of convective water flow through a micro-tube. The effects of variation in inlet temperature and wall heat flux on heat transfer are studied for variable fluid properties. The results show that the Nu decreases with an increase in inlet temperature for variable fluid properties. The deviations produced by temperature-dependent properties on heat transfer and frictional flow characteristics of water flowing through a microchannel are numerically investigated by Kumar and Mahulikar [25]. The Nu displays a significant deviation from conventional theory due to flattening of the radial temperature profile due to thermal conductivity variation. The performance of the heat sink is optimized with the help of the entropy generation minimization (EGM) method [26-28].

Kumar and Mahulikar [29] and Kumar [30] analyzed the rarefaction and non-rarefaction effects on heat transfer characteristics of hydrodynamically and thermally developing airflow through microtubes. Keepaiboon et al. [31] experimental investigated boiling heat transfer characteristics of a refrigerant in a microfluidic channel at a high mass flux. They proposed the new boiling heat transfer correlation of a refrigerant for two-phase flow at the microfluidic scale Gaikwad et al. [32] discussed the EGM in a slip-modulated electrically actuated transport through an asymmetrically heated microchannel. Optimum values of geometric and thermo-physical parameters were introduced for which a change in the thermal transport of heat caused by viscous dissipation and Joule heating effect leads to EGM in the system. Sarma et al. [33] analyzed the entropy generation characteristics under the influence of interfacial slip for a non-Newtonian microflow. The optimum value of the geometric parameter such as the channel wall thickness and the thermophysical parameters such as the Peclet number (Pe) and Biot number (Bi), were determined, leading to a minimum rate of entropy generation in the system. Sarma et al. [34] examined the prominent role of the Debye–Hückel parameter, viscoelastic parameter, the thermal conductivity of the wall, channel wall thickness, Bi, Pe, and axial temperature gradient on the entropy generation rate. They established the optimum values of the above parameters, leading to the EGM method.

OBJECTIVE AND SCOPE OF INVESTIGATION

The important step for the analysis of water cooling with forced convection is the use of a similar argument, the Reynolds analogy. The Reynolds analogy is a powerful analytical tool since it was first proposed in the late 1800s. This states that the f_f due to fluid flowing over the wall is proportional to the convective heat transfer coefficient (h). It's most simple form is, $St = f_f/2$ for CFP. Earlier, the Reynolds analogy is valid for incompressible and laminar flows. It has been extended to turbulent flows in different computational as well as analytical forms by many researchers. Mahulikar and Herwig [9] reported that the effect of $\mu(T)$ and $k(T)$ variations for water is highly significant in micro-convection. Gulhane and Mahulikar [18] and Kumar and Mahulikar [35] reported that the effect of $\rho(T)$ variation for water is significant in micro-convection due to a rapid increment in fluid bulk mean temperature. Therefore, the

present research is an extension of the earlier work reported by Kumar and Mahulikar [23], to include the effect of $\rho(T)$ variation in addition to $\mu(T)$ and $k(T)$ variations. Hence, the first objective of the present research is to reexamine the Reynolds analogy for the case of combined $\rho(T)$, $\mu(T)$, and $k(T)$ variations without entrance effect. Due to TFP, three modified non-dimensional parameters "$\Pi_{S\rho T}$, $\Pi_{S\mu T}$, and Π_{SkT}" are emerged from the dimensionless form of governing conservation equations. The role of $\Pi_{S\mu T}$ and Π_{SkT} in flow friction was analyzed by Kumar and Mahulikar [23]. It is also thought that in micro-convection, $\Pi_{S\rho T}$ creates a powerful impact on flow friction. Therefore, the second objective of the investigation is to examine the role of $\Pi_{S\rho T}$, $\Pi_{S\mu T}$, and Π_{SkT} in flow friction. The Poiseuille number ($Po = 4\,f_f{\cdot}Re_D$) correlates with $\Pi_{S\rho T}$, $\Pi_{S\mu T}$, and Π_{SkT} to find the effects of TFP on laminar liquid micro-convection. This research would be very helpful in improving micro-convection knowledge that offers better efficiency of micro-devices.

DESCRIPTION OF THE PROBLEM

A circular cross-sectional micro-tube with an aspect ratio (L/D) = 50 is subjected to constant wall heat flux (CWHF) boundary condition (BC) as shown in figure 1. The following data is fixed for all investigated cases: Radius of micro-tube $R = 50 \times 10^{-6}$ m, length of micro-tube $L = 5 \times 10^{-3}$ m, and inlet temperature at axis $T_{0,in} = 293$ K. The smaller diameter and higher aspect ratio are selected to analyze the effect of steeper temperature gradients on laminar microconvection characteristics.

Problem Formulation

Attention is focused on the calculation of *St*, *Nu*, *Re*, Prandtl number (*Pr*), Peclet number (*Pe*), *Po* given as: $St = h/(\rho_m{\cdot}u_m{\cdot}c_p)$, $Nu = h{\cdot}D/k_m$, $Re = \rho_m{\cdot}u_m{\cdot}D/\mu_m$, $Pr = c_p{\cdot}\mu_m/k_m$, $Pe = Re{\cdot}Pr$, $Po = 4f_f{\cdot}Re_D$. The subscript 'm' shows the mean value of the properties evaluated at bulk mean temperature (T_m). The cross-sectionally weighted averaged axial velocity (mean velocity) u_m is defined as [17]: $u_m = \dfrac{\int_A \rho{\cdot}u(r){\cdot}dA}{\rho{\cdot}A}$ ($1/\rho{\cdot}A$) and T_m is the enthalpy-average temperature (bulk mean temperature) of the bulk fluid, which represents the total energy of the flow at a reference point as [17]: $T_m = \int_0^R \rho(r){\cdot}u(r){\cdot}T(r){\cdot}r{\cdot}dr \,/ \int_0^R \rho(r){\cdot}u(r){\cdot}r{\cdot}dr$ for constant c_p. The *St* is also known as modified *Nu* and it can also be expressed in terms of the *Nu*, *Re*, *Pr*, and *Pe* as: $St = Nu/(Re{\cdot}Pr) = Nu/Pe$. The f_f is defined as the ratio of wall shear stress (τ_w) to dynamic pressure $\left(\rho_m \cdot u_m^2/2\right)$ as: $f_f = \tau_w / \left(\rho_m \cdot u_m^2/2\right)$, where $\tau_w = \mu_w{\cdot}(\partial u/\partial r)_w$. For laminar FDF with CFP, $f_f{\cdot}Re_D = 16$ and $Po = 64$. Therefore, *St* can be written as:

$$St = \left[\frac{Nu}{16{\cdot}Pr}\right] f_f \tag{1}$$

From this relation, it is concluded that *St* increases with an increase in f_f. Therefore, the Reynolds analogy is popularly regarded as holding when *St* increases for CFP with an increase in f_f. The Reynolds analogy valid region illustrates the region in which convective HT is more emphatic at the cost of augmented f_f. As per Reynolds analogy, the flattening of velocity profile improves *St* and *Nu*, it also increases f_f. However, the flattening or sharpening of the velocity profile is affected due to TFP, which affects *Nu* [10]. It was supposed that the Reynolds analogy was invalid for liquids (when $Pr \neq 1$) and particularly when TFP were considered [36]. Therefore, the Reynolds analogy is revisited for TFP. From the study of Gulhane and Mahulikar [18], It is found that *h* increases as a result of flattening the velocity profile,

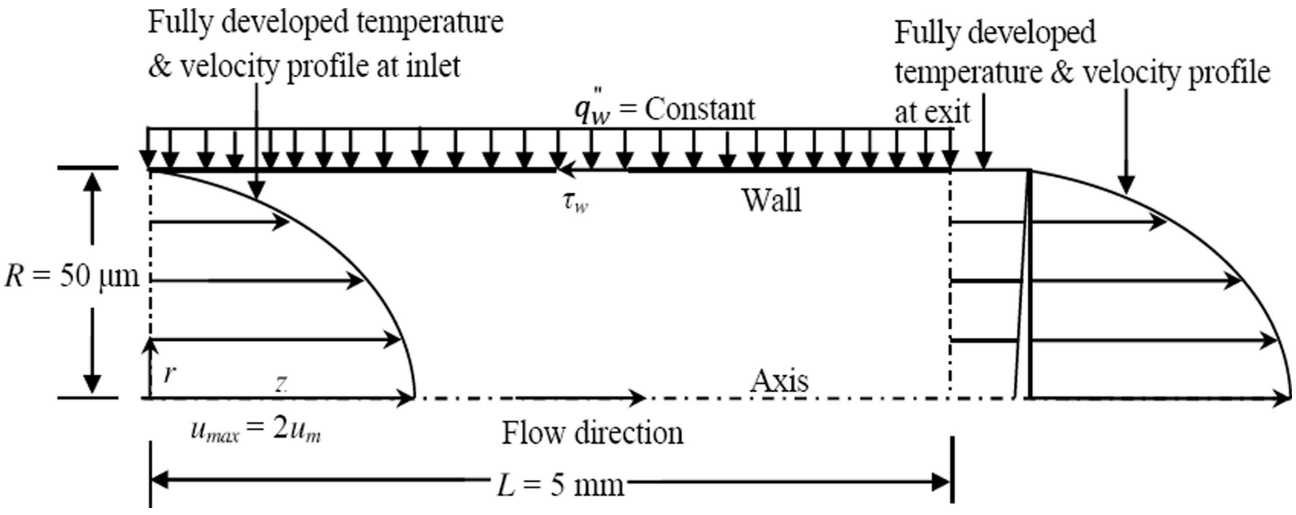

Figure 1. Schematic of 2D (with axisymmetry) circular micro-channel with the constant wall heat flux boundary condition.

which increases *St* along the flow. The flattening of the velocity profile results in radially outward flow, which can not be ignored, and radial convection has a significant effect on convective HT, because $Nu\ \alpha\ (\partial u/\partial r)_w$. Owing to flattening of $u(r, z)$ profile, $(\partial u/\partial r)_w$ increases, therefore *Nu* also increases [10]. Due to TFP, $\tau_w\ \alpha\ \mu_m$ [15]. The reduction in μ_m along the flow causes a reduction in f_f, when Reynolds analogy is valid. Hence, Reynolds analogy is now valid when *St* increases with a reduction in f_f for TFP. It is concluded that the Reynolds analogy helps to find the flow regime in which *h* increases while τ_w decreases for TFP. By putting $St = Nu/(Re{\cdot}Pr)$ in equation (1), can be written in this form: $(1/Re) = (f_f/16)$. Therefore, the Reynolds analogy is qualitatively valid for that region, where $(1/Re)$ and f_f are directly dependent.

Governing Equations

The following 2-dimensional, steady-state, laminar, continuum-based governing conservation equations in cylindrical coordinates (with axisymmetry) incorporating $\rho(T)$, $\mu(T)$, and $k(T)$ variations in dimensional and nondimensional forms, as elaborated in Gulhane and Mahulikar [18] are numerically solved.

Continuity equation

Dimensional form

$$\left(v\cdot\frac{\partial\rho}{\partial r}\right)+\rho\left[\left(\frac{\partial u}{\partial z}\right)+\left(\frac{v}{r}\right)+\left(\frac{\partial v}{\partial r}\right)\right]+\left(u\cdot\frac{\partial\rho}{\partial z}\right)=0 \quad (2)$$

Non dimensional form

$$\overline{S}_{\rho T}\cdot\Pi_{S\rho T}\cdot\left(\overline{v}\cdot\frac{\partial\theta}{\partial\overline{r}}+\frac{1}{2}\overline{u}\cdot\frac{\partial\theta}{\partial\overline{z}}\right)+\overline{\rho}\left(\frac{\overline{v}}{\overline{r}}+\frac{\partial\overline{v}}{\partial\overline{r}}+\frac{1}{2}\frac{\partial\overline{u}}{\partial\overline{z}}\right)=0 \quad (3)$$

Momentum equation [Axial direction]

Dimensional form

$$\rho\cdot\left(v\cdot\frac{\partial u}{\partial r}+u\cdot\frac{\partial u}{\partial z}\right)=-\frac{\partial p}{\partial z}+\left[\left(\frac{\mu}{r}+\frac{\partial\mu}{\partial r}\right)\cdot\left(\frac{\partial u}{\partial r}\right)\right]$$
$$+\mu\cdot\left[\left(\frac{\partial^2 u}{\partial z^2}\right)+\left(\frac{\partial^2 u}{\partial r^2}\right)\right]+\left(\frac{\partial\mu}{\partial z}\right)\cdot\left(\frac{\partial u}{\partial z}\right) \quad (4)$$

Nondimensional form

$$\overline{\rho}\cdot Re_D\left(2\overline{v}\cdot\frac{\partial\overline{u}}{\partial\overline{r}}+\overline{u}\cdot\frac{\partial\overline{u}}{\partial\overline{z}}\right)=-\left(\frac{\partial\overline{p}}{\partial\overline{z}}\right)+\left(\overline{S}_{\mu T}\cdot\Pi_{S\mu T}\right)$$
$$\left[4\cdot\left(\frac{\partial\theta}{\partial\overline{r}}\right)\cdot\left(\frac{\partial\overline{u}}{\partial\overline{r}}\right)+\left(\frac{\partial\theta}{\partial\overline{z}}\right)\cdot\left(\frac{\partial\overline{u}}{\partial\overline{z}}\right)\right]$$
$$+\overline{\mu}\cdot\left[\frac{4}{\overline{r}}\cdot\left(\frac{\partial\overline{u}}{\partial\overline{r}}\right)+4\cdot\left(\frac{\partial^2\overline{u}}{\partial\overline{r}^2}\right)+\frac{\partial^2\overline{u}}{\partial\overline{z}^2}\right] \quad (5)$$

Momentum equation [Radial direction]

Dimensional form

$$\rho\cdot\left(v\cdot\frac{\partial v}{\partial r}+u\cdot\frac{\partial v}{\partial z}\right)=-\frac{\partial p}{\partial r}+\left[\left(\frac{\partial\mu}{\partial r}-\frac{\mu}{r}\right)\right]\cdot\left(\frac{v}{r}\right)$$
$$+\mu\cdot\left[\left(\frac{\partial^2 v}{\partial z^2}\right)+\left(\frac{\partial^2 v}{\partial r^2}\right)\right]+\left(\frac{\partial\mu}{\partial z}\right)\cdot\left(\frac{\partial v}{\partial z}\right)$$
$$+\left[\left(\frac{\mu}{r}+\frac{\partial\mu}{\partial r}\right)\cdot\left(\frac{\partial v}{\partial r}\right)\right] \quad (6)$$

Nondimensional form

$$\overline{\rho}\cdot Re_D\left(2\overline{v}\cdot\frac{\partial\overline{v}}{\partial\overline{r}}+\overline{u}\cdot\frac{\partial\overline{v}}{\partial\overline{z}}\right)=-2\left(\frac{\partial\overline{p}}{\partial\overline{r}}\right)+\left(\overline{S}_{\mu T}\cdot\Pi_{S\mu T}\right)$$
$$\left[4\cdot\left(\frac{\partial\theta}{\partial\overline{r}}\right)\left[\frac{\overline{v}}{\overline{r}}+\frac{\partial\overline{v}}{\partial\overline{r}}\right]+\left(\frac{\partial\theta}{\partial\overline{z}}\right)\cdot\left(\frac{\partial\overline{v}}{\partial\overline{z}}\right)\right]$$
$$+\overline{\mu}\cdot\left[\frac{4}{\overline{r}}\cdot\left(\frac{\partial\overline{v}}{\partial\overline{r}}\right)-4\cdot\left(\frac{\overline{v}}{\overline{r}^2}\right)+\left(\frac{\partial^2\overline{v}}{\partial\overline{z}^2}\right)+4\cdot\left(\frac{\partial^2\overline{v}}{\partial\overline{r}^2}\right)\right] \quad (7)$$

Energy equation

Dimensional form

$$\rho\cdot c_p\cdot\left(v\cdot\frac{\partial T}{\partial r}+u\cdot\frac{\partial T}{\partial z}\right)=\left[\frac{k}{r}+\frac{\partial k}{\partial r}\right]\cdot\left(\frac{\partial T}{\partial r}\right)$$
$$+k\cdot\left(\frac{\partial^2 T}{\partial r^2}\right)+\left(\frac{\partial k}{\partial z}\right)\cdot\left(\frac{\partial T}{\partial z}\right)+k\cdot\left(\frac{\partial^2 T}{\partial r^2}\right)+$$
$$\mu\cdot\left\{\left[\left(\frac{\partial v}{\partial z}+\frac{\partial u}{\partial r}\right)\right]^2+\left(\frac{4}{3}\right)\cdot\left[\begin{array}{l}\left(\frac{\partial v}{\partial r}\right)^2+\left(\frac{v}{r}\right)^2+\left(\frac{\partial u}{\partial z}\right)^2\\ -\left(\frac{\partial v}{\partial r}\right)\cdot\left(\frac{v}{r}\right)-\\ \left(\frac{\partial v}{\partial r}\right)\cdot\left(\frac{\partial u}{\partial z}\right)-\left(\frac{v}{r}\right)\cdot\left(\frac{\partial u}{\partial z}\right)\end{array}\right]\right\} \quad (8)$$

Nondimensional form

$$\overline{\rho}\left(2\cdot\overline{v}\cdot\frac{\partial\theta}{\partial\overline{r}}+\overline{u}\cdot\frac{\partial\theta}{\partial\overline{z}}\right)=\frac{\overline{k}}{Pe_D}\left(4\left(\frac{1}{\overline{r}}\cdot\frac{\partial\theta}{\partial\overline{r}}+\frac{\partial^2\theta}{\partial\overline{z}^2}\right)+\frac{1}{2}\cdot\frac{\partial^2\theta}{\partial\overline{z}^2}\right)$$
$$+\frac{\Pi_{SkT}\cdot\overline{S}_{kT}}{Pe_D}\left(4\left(\frac{\partial\theta}{\partial\overline{r}}\right)^2+\left(\frac{\partial\theta}{\partial\overline{z}}\right)^2\right)+4\left(\frac{Br_{qw}}{Pe_D}\right)$$
$$\overline{\mu}\left\{\cdot\left[\left(\frac{1}{2}\cdot\frac{\partial\overline{v}}{\partial\overline{z}}\right)+\left(\frac{\partial\overline{u}}{\partial\overline{r}}\right)\right]^2+\frac{4}{3}\overline{\mu}\left[\begin{array}{l}\left(\frac{\partial\overline{v}}{\partial\overline{r}}\right)^2+\left(\frac{\overline{v}}{\overline{r}}\right)^2\\ +\left(\frac{1}{4}\cdot\frac{\partial\overline{u}}{\partial\overline{z}}\right)^2-\left(\frac{\partial\overline{v}}{\partial\overline{r}}\right)\\ \cdot\left(\frac{\overline{v}}{\overline{r}}\right)-\frac{1}{2}\left(\frac{\partial\overline{v}}{\partial\overline{r}}\right)\cdot\left(\frac{\partial\overline{u}}{\partial\overline{z}}\right)\\ -\frac{1}{2}\left(\frac{\overline{v}}{\overline{r}}\right)\cdot\left(\frac{\partial\overline{u}}{\partial\overline{z}}\right)\end{array}\right]\right\} \quad (9)$$

The non-dimensional static pressure and non-dimensional temperature are given as $\bar{p} = p{\cdot}D/(\mu_m{\cdot}u_m)$ and $\theta = k_m{\cdot}(T{-}T_m)/(q''_w{\cdot}D)$ respectively. The $S_{\rho T}$ $(= \partial\rho/\partial T)$ is the density-temperature sensitivity, $S_{\mu T}$ $(= \partial\mu/\partial T)$ is the viscosity-temperature sensitivity and S_{kT} $(= \partial k/\partial T)$ is the thermal-conductivity-temperature sensitivity. The Re_D and Pe_D are *Re* and *Pe* based on diameter respectively. The laminar micro-convective flow with TFP depends upon the following non-dimensional parameters: Br_{qw} $[= \mu_m{\cdot}u_m^2/(q''_w{\cdot}D)$, $\Pi_{S\rho T}$ $[=|Br_{S\rho T}/Br_{qw}|]$, $\Pi_{S\mu T}$ $[=|Br_{S\mu T}/Br_{qw}|]$, Π_{SkT} $[=|Br_{SkT}/Br_{qw}|]$. The Π parameters are the magnitude of the product of the temperature perturbation parameter $[= f(q''_w{\cdot}D/k)]$ and non-dimensional property sensitivities, $S_{\rho T}(T/\rho)$, $S_{\mu T}(T/\mu)$ *and* $S_{kT}(T/k)$. The modified non-dimensional parameter "$\Pi_{S\rho T}$" shows the comparative importance of momentum transport due to $S_{\rho T}$ over energy transport due to fluid conduction. The "$\Pi_{S\mu T}$" indicates the significance of cross-flow momentum transport over energy transport due to $S_{\mu T}$. The Π_{SkT} gives the comparative importance of momentum transport due to S_{kT} and energy flow due to fluid conduction. Higher values of Π parameters show a stronger influence on micro-convection due to temperature-dependent fluid properties. The Brinkman number "Br_{qw}" appears in the non-dimensional energy equation as the product of *Pr* and Eckert numbers (*Ec*). $Br_{qw} = Pr{\cdot}Ec = \mu_m{\cdot}u_m^2/(k_m{\cdot}\Delta T)$, where $\Delta T = (T_w{-}T_m)$. The $Br_{S\rho T}$ $[= S_{\rho Tm}{\cdot}u_m^2{\cdot}\mu_m/(\rho_m{\cdot}k_m)]$ is the modified *Br* based on $S_{\rho T}$. The $Br_{S\mu T}$ $[= S_{\mu Tm}{\cdot}u_m^2/k_m]$ is the modified *Br* based on $S_{\mu T}$. The Br_{SkT} $[= S_{kTm}{\cdot}u_m^2{\cdot}\mu_m/k_m^2]$ is the modified *Br* based on S_{kT} [9]. The other non-dimensional parameters are involved in the governing equations as:

$\tilde{z} = z/D$	$\tilde{r} = r/R$	$\tilde{\rho} = \rho/\rho_m$	$\tilde{\mu} = \mu/\mu_m$	$\tilde{k} = k/k_m$
$\tilde{u} = u/u_m$	$\tilde{v} = v/u_m$	$\tilde{S}_{\rho T} = S_{\rho T}/S_{\rho Tm}$	$\tilde{S}_{\mu T} = S_{\mu T}/S_{\mu Tm}$	$\tilde{S}_{kT} = S_{kT}/S_{kTm}$

Boundary Conditions

The computational field is subjected to four flow and thermal boundary conditions (BCs) as follows:

1. Inlet ($z = 0$): The laminar, FDF profiles of $u(r)$ and $T(r)$ at the inlet-upstream for CFP are given as: $u_{in}(r) = 2u_{m,in}(1{-}\tilde{r}^2)$ and $T_{in}(r) = T_{0,in} + (q''_w{\cdot}R/k){\cdot}[\tilde{r}^2{-}(\tilde{r}^4/4)]$ respectively [37]. The $u_{m,in}$ is the inlet mean axial velocity and $T_{0,in}$ is the inlet water temperature at the axis. The variations in $\rho(T)$, $\mu(T)$ and $k(T)$ are turned on from inlet downstream ($z = 0^+$). The influence of thermophysical properties on micro-convective flow without considering entrance effects is expressed by this inlet BC [10]. The present study focuses primarily on the effects of fluid thermophysical properties on micro-convective flow only. Thus, the entrance effects are ignored. However, in general, the micro-convection characteristics are determined jointly by taking into account the effects of the entrance and fluid thermophysical properties.
2. Outlet ($z = L$): $p_{ex} = 1.01325{\times}10^5$ Pa (atmospheric pressure) and $v_{ex} = 0$ since, $\partial u/\partial z = 0$.
3. Axis ($r = 0$): The BC of symmetry is imposed at the axis of tube; hence, $(\partial u/\partial r) = (\partial p/\partial r) = (\partial T/\partial r) = (\partial\rho/\partial r) = 0$.
4. Wall ($r = R$): No-slip and no normal flow BCS are imposed at the nonporous rigid wall of the tube; therefore, $u_w = v_w = 0$. The constant is applied at the wall, $q''_w = k_w{\cdot}(\partial T/\partial r)_w$.

Computational Domain and Numerical Methodology

The computational field is split into the graded mesh [10,000 cells = 200 (in the axial direction) × 50 (in the radial direction)] with a finer grid spacing near the inlet and the wall. The finer grid spacing near the inlet and the wall is used to capture a rapid change in fields of temperature and flow. The governing equations (2)-(9) with BCs are solved by ANSYS FLUENT software. FLUENT is based on a finite volume differencing scheme which is 2nd-order accurate. The algorithm "Semi-Implicit Method For Pressure-Linked Equations" (SIMPLE) is used to achieve a good convergence behavior. When the residuals for continuity, *r*, and *z* momentum equations are less than 10^{-12} and less than 10^{-15} for the energy equation, the solution is deemed converged. Additional information related to the accuracy of the numerical results, the convergence of solution, and validation with benchmark cases for CFP are in [10, 15, and 23].

RESULTS AND DISCUSSION

Inference from Theoretical Studies based on TFP

For water in the temperature range of 273-373 K, the variations in $\rho(T)$, $\mu(T)$, and $k(T)$ are 4%, 84%, and 21% respectively [38]. The $\rho(T)$ variation for pure water in the temperature range of 274-372 K is given by the Thiesen-Scheel-Diesselhorst relation as [39]:

$$\rho(T) = 1000{\cdot}\left[1 - \frac{(T+288.9414){\cdot}(T-3.9863)^2}{508929.2{\cdot}(T+68.12963)}\right]\frac{kg}{m^3} \quad (10)$$

where *T* is in °C. The pressure effect on density is normally ignored in the case of water. The $\mu(T)$ variation for single-phase water is given as [40]:

$$\mu(T) = \mu(T_{ref}){\cdot}\left(\frac{T}{T_{ref}}\right)^n{\cdot}\exp\left[B{\cdot}\left(\frac{1}{T} - \frac{1}{T_{ref}}\right)\right]\frac{kg}{m{\cdot}s} \quad (11)$$

where $n = 8.9$, $B = 4{,}700$, $\mu(T_{ref}) = 1.005{\times}10^{-3}$ kg/ms, $T_{ref} = 293$ K.

The $k(T)$ variation for single-phase water is calculated by least-squares error third-order polynomial fitting of data in the operating temperature range of 274-372 K as [38]:

$$k(T)=\begin{bmatrix}-1.51721+0.0151476\cdot T-3.5035\\ \times10^{-5}\cdot T^{2}+2.74269\times10^{-8}\cdot T^{3}\end{bmatrix}\frac{W}{m\cdot K} \quad (12)$$

The $c_p(T)$ variation is less than 1% within a temperature range of 274-372 K, hence, c_p is assumed to be constant. The micro-convective flow has the following characteristics:

(1) *Density-temperature sensitivity*

$$S_{\rho T}=\left(\frac{\partial\rho}{\partial T}\right)=-1000\cdot\begin{bmatrix}(508929.2\cdot T+34673158.1)\\ \cdot\begin{Bmatrix}2\cdot(T-3.9863)\cdot(T+288.9414)\\ +(T-3.9863)^{2}\end{Bmatrix}\\ -508929.2\cdot(T-3.9863)^{2}\cdot(T+288.9414)\end{bmatrix}\Big/(508929.2\cdot T+34673158.1)^{2} \quad (13)$$

$$\frac{kg}{m^{3}\cdot{}^{\circ}C}$$

The $S_{\rho T}>0$ for 0 to 4 °C, because water density increases with increasing temperature. However, after 4 °C, $S_{\rho T}<0$ is negative because water density decreases with increasing temperature.

(2) *Viscosity-temperature sensitivity*

$$S_{\mu T}=\left(\frac{\partial\mu}{\partial T}\right)=T^{n-1}\cdot\exp\left[B\cdot\left(\frac{1}{T}-\frac{1}{T_{\text{ref}}}\right)\right]\cdot10^{-22}\left(0.0099182-\frac{5.2377}{T}\right)\frac{kg}{m\cdot s\cdot K}(<0) \quad (14)$$

In liquids, water has very high $S_{\mu T}$. The $S_{\mu T}<0$ since water viscosity decreases with increasing temperature.

(3) *Thermal conductivity-temperature sensitivity*

$$S_{kT}=(\partial k/\partial T)=\begin{bmatrix}0.0151476-7.007\\ \times10^{-5}\cdot T+8.22807\\ \times10^{-8}\cdot T^{2}\end{bmatrix}\frac{W}{m\cdot K^{2}}(>0) \quad (15)$$

The $S_{kT}>0$ as water thermal conductivity increases with increase in temperature. The profiles of $v(r, z)$, $u(r, z)$, and $T(r, z)$ are produced and the variations of St, f_f, Re, and Pr along the flow are examined for the case of combined $\rho(T)$, $\mu(T)$ and $k(T)$ variations. Table 1 gives $f_{f,in}$, $f_{f,max}$, and $f_{f,ex}$, Re_{in} and Re_{ex}, St_{in} and St_{ex}, and $\bar{z}_{ff,max}$, for $u_{m,in}$ = 0.075, 0.5, 1, 2, and 3 m/s, for different allowable .

Figure 2 shows St versus f_f for $u_{m,in}$ = 0.075, 1, and 3 m/s, for different allowable q''_w; for observing the validity of the Reynolds analogy. The St increases along the flow and f_f depends upon τ_w. Firstly the f_f increases and attains its maximum value ($f_{f,max}$) at axial location $z_{ff,max}$, and then decreases as shown in Figure 4. From equation (1), St α f_f for CFP. Therefore, in general, the Reynolds analogy is supposed to be valid when St increases with an increase in f_f for CFP. However, for micro-convective flow with TFP, the validity of the Reynolds analogy results in an increase in St with a decrease in f_f. The flow regime in which St increases with decreasing f_f is significant for the case of $u_{m,in}$ = 0.075 m/s. Therefore, Reynolds analogy is largely valid for $u_{m,in}$ = 0.075 m/s as shown in figure 2(a). As $u_{m,in}$ increases, the flow regime in which St increases with decreasing f_f reduces. Hence, Reynolds analogy valid region also reduces for $u_{m,in}$ = 1 m/s as illustrated in Figure 2(b). A smaller flow regime in which St increases with decreasing f_f is observed in the case of $u_{m,in}$ = 3 m/s. Therefore, the Reynolds analogy is largely invalid for $u_{m,in}$ = 3 m/s as shown in Figure 2(c).

Figure 3 illustrates $(1/Re)$ versus f_f, for the same cases as taken in figure 2, which shows reversed patterns of variations of $(1/Re)$ versus f_f and St versus f_f. From figure 3(a), it is observed that $(1/Re)$ and f_f are directly proportional over a larger flow regime. Therefore, Reynolds analogy is largely valid for $u_{m,in}$ = 0.075 m/s. As $u_{m,in}$ increases, the flow regime in which $(1/Re)$ and f_f are directly proportional reduces as clearly illustrated in figures 3(b, c). Figure 3(c) shows that the Reynolds analogy is invalid for a larger flow regime in the case of $u_{m,in}$ = 3 m/s. Figure 4 shows f_f versus z/D. Firstly f_f increases rapidly along the flow and the maximum value of f_f (= $f_{f,max}$) reaches at the axial location $\bar{z}_{ff,max}$ and after that, f_f decreases along the flow as shown in figure 4. The following reasons are attributed to this, (1) The flow undevelopment happens in the locality of the inlet due to $\mu(T)$ variation as $\partial/\partial z(\partial u/\partial r)_w > 0$. (2) The water viscosity reduces with increasing temperature which decays f_f along the flow as $(\partial\mu/\partial z) < 0$ [18]. As q''_w increases, the axial location $\bar{z}_{ff,max}$ moves towards the exit of micro-tube for same $u_{m,in}$ as given in Table 1 and also shown in Figure 4.

The variation of Po along the flow is illustrated in figure 5. It is observed that Po decreases with increasing q''_w and $u_{m,in}$. The main cause behind this is: the rate of increase in Re is less than the rate of reduction in f_f. It is also noted that the rate of change of Re increases with an increase in q''_w, which is confirmed from Table 1. The deviation in Po from 64 is smaller in the locality of the inlet for the case of lower q''_w as illustrated in Figure 5(a). As q''_w increases, the deviation in Po from 64 also increases which is clearly shown in figures 5(a, b, c).

Significance of the modified non-dimensional parameters, $\Pi_{S\rho T}$, $\Pi_{S\mu T}$, and Π_{SkT}

Three modified non-dimensional parameters "$\Pi_{S\rho T}$, $\Pi_{S\mu T}$, and Π_{SkT}" appear from the dimensionless form of

Table 1. Variation in convective flow parameter with $u_{m,in}$ and q''_w

$u_{m,in}$ (m/s)	q''_w (W/cm²)	Re_{in}	Re_{ex}	$f_{f,in}$	$f_{f,max}$	$f_{f,ex}$	St_{in}	St_{ex}	$\bar{z}_{ff,max}$
	1.5	7.49	9.38	2.0799	2.1104	1.6945	0.0856	0.0977	0.3214
0.075	3	7.55	11.51	2.0357	2.0705	1.3745	0.0856	0.1002	0.3214
	6	7.69	16.32	1.9513	1.9941	0.9636	0.0856	0.1043	0.3214
	7.5	51.76	61.19	0.2857	0.2949	0.2530	0.0128	0.0135	1.6475
	15	54.03	73.92	0.2580	0.2711	0.2045	0.0128	0.0139	1.7431
0.5	30	58.71	102.39	0.2133	0.2315	0.1432	0.0129	0.0145	1.8397
	60	68.59	166.17	0.1536	0.1754	0.0868	0.0129	0.0152	2.1353
	90	79.09	228.28	0.1175	0.1386	0.0644	0.0130	0.0154	2.3374
	30	117.45	158.64	0.1064	0.1159	0.0908	0.0064	0.0070	3.6378
	60	137.19	229.26	0.0765	0.0878	0.0601	0.0065	0.0074	4.1069
	90	158.14	305.97	0.0585	0.0695	0.0445	0.0065	0.0076	4.5951
1	120	180.09	382.98	0.0471	0.0569	0.0360	0.0065	0.0077	5.1032
	150	202.79	454.90	0.0396	0.0481	0.0311	0.0065	0.0078	5.4977
	180	225.99	517.53	0.0345	0.0418	0.0283	0.0065	0.0078	6.0423
	90	316.27	457.87	0.0292	0.0348	0.0282	0.0032	0.0037	8.9473
	120	360.13	558.63	0.0235	0.0285	0.0229	0.0032	0.0038	9.9847
	150	405.49	660.89	0.0198	0.0241	0.0194	0.0032	0.0039	10.8978
2	180	451.85	761.21	0.0172	0.0209	0.0172	0.0033	0.0039	11.8576
	210	498.72	856.48	0.0155	0.0187	0.0157	0.0033	0.0039	12.8662
	240	545.60	944.12	0.0142	0.0170	0.0147	0.0033	0.0039	13.9263
	270	592.00	1022.11	0.0134	0.0158	0.0142	0.0033	0.0040	15.0405
	90	474.43	613.13	0.0195	0.0232	0.0206	0.0022	0.0025	13.4960
	120	540.19	735.21	0.0157	0.0190	0.0168	0.0022	0.0025	14.8132
	150	608.21	860.91	0.0132	0.0161	0.0143	0.0022	0.0026	16.2116
3	180	677.74	987.12	0.0115	0.0140	0.0126	0.0022	0.0026	17.6959
	210	748.03	1110.86	0.0103	0.0124	0.0114	0.0022	0.0026	19.2716
	240	818.32	1229.45	0.0095	0.0113	0.0106	0.0022	0.0026	20.9442
	270	887.92	1340.56	0.0089	0.0105	0.0100	0.0022	0.0026	22.7197

governing conservation equations [Ref. Eqs. (3), (5), (7), and (9)]. Following dimensional analysis shows the dependence of the f as,

$$f = \phi\left(\rho, u_m, D, \mu, k, S_{\rho T}, S_{\mu T}, S_{kT}, q''_w\right) \tag{16}$$

The dimensions of the nine parameters are: $[\rho] = [M^1L^{-3}]$, $[u_m] = [L^1T^{-1}]$, $[D] = [L^1]$, $[\mu] = [M^1L^{-1}T^{-1}]$, $[k] = [M^1L^1T^{-3}\Theta^{-1}]$, $[S_{\rho T}] = [M^1L^{-3}\Theta^{-1}]$ $[S_{\mu T}] = [M^1L^{-1}T^{-1}\Theta^{-1}]$, $[S_{kT}] = [M^1L^1T^{-3}\Theta^{-2}]$ and $[q''_w] = [M^1T^{-3}]$. The M, L, T, and Θ are the primary dimensions of mass, length, time, and temperature, respectively. There is a total of nine variables ($n = 9$) in equation (16) and 4 primary dimensions ($m = 4$), hence, according to the Buckingham-Π theorem, there are 5 (n–m) independent non-dimensional groups. Selecting ρ, u_m, D and k as the repeating variables (RV) and leaving the remaining parameters as; μ, $S_{\rho T}$, $S_{\mu T}$, S_{kT} and q''_w, five non-dimensional groups are obtained as follows: $\Pi_1 = Re_D = \rho \cdot u_m \cdot D/\mu$, $\Pi_2 = Br_{qw} = \mu \cdot u^2{}_m/(q''_w \cdot D)$, $\Pi_3 = Br_{S\rho T} = S_{\rho T} \cdot u^2{}_m \cdot \mu/(\rho \cdot k)$, $\Pi_4 = Br_{S\mu T} = S_{\mu T} \cdot u^2{}_m/k$, $\Pi_5 = Br_{SkT} = S_{kT} \cdot \mu \cdot u^2{}_m/k^2$. The Br_{qw} is Br based on q''_w, $Br_{S\rho T}$ is modified Br based on $S_{\rho T}$; and $\Pi_{S\rho T} = |Br_{S\rho T}/Br_{qw}| = |S_{\rho T} \cdot q''_w \cdot D/(\rho \cdot k)|$, $Br_{S\mu T}$ is modified Br based on $S_{\mu T}$; and $\Pi_{S\mu T} = |Br_{S\mu T}/Br_{qw}| = |S_{\mu T} \cdot q''_w \cdot D/(\mu \cdot k)|$ and Br_{SkT} is modified Br based on S_{kT}; and $\Pi_{SkT} = |Br_{SkT}/Br_{qw}| = |S_{kT} \cdot q''_w \cdot D/k^2|$ [9]. The dimensionless form of the governing equations and above dimensional analysis gives a short form of equation (16) as, $f = \phi(Re_D, \Pi_{S\rho T}, \Pi_{S\mu T}, \Pi_{SkT})$.

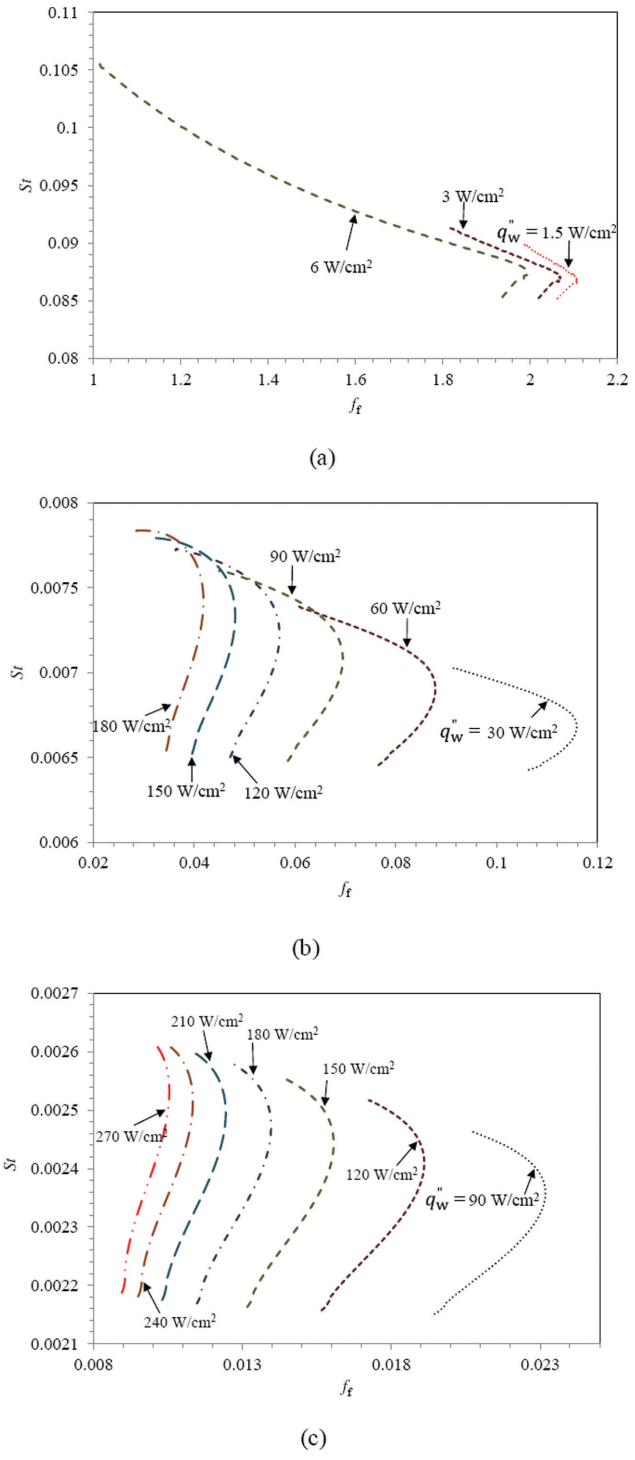

Figure 2. Variation of *St* versus f_f: Examination of Reynolds' analogy: (a) $u_{m,in}$ = 0.075 m/s (Reynolds' analogy largely valid), (b) $u_{m,in}$ = 1 m/s, and (c) $u_{m,in}$ = 3 m/s (Reynolds' analogy largely invalid).

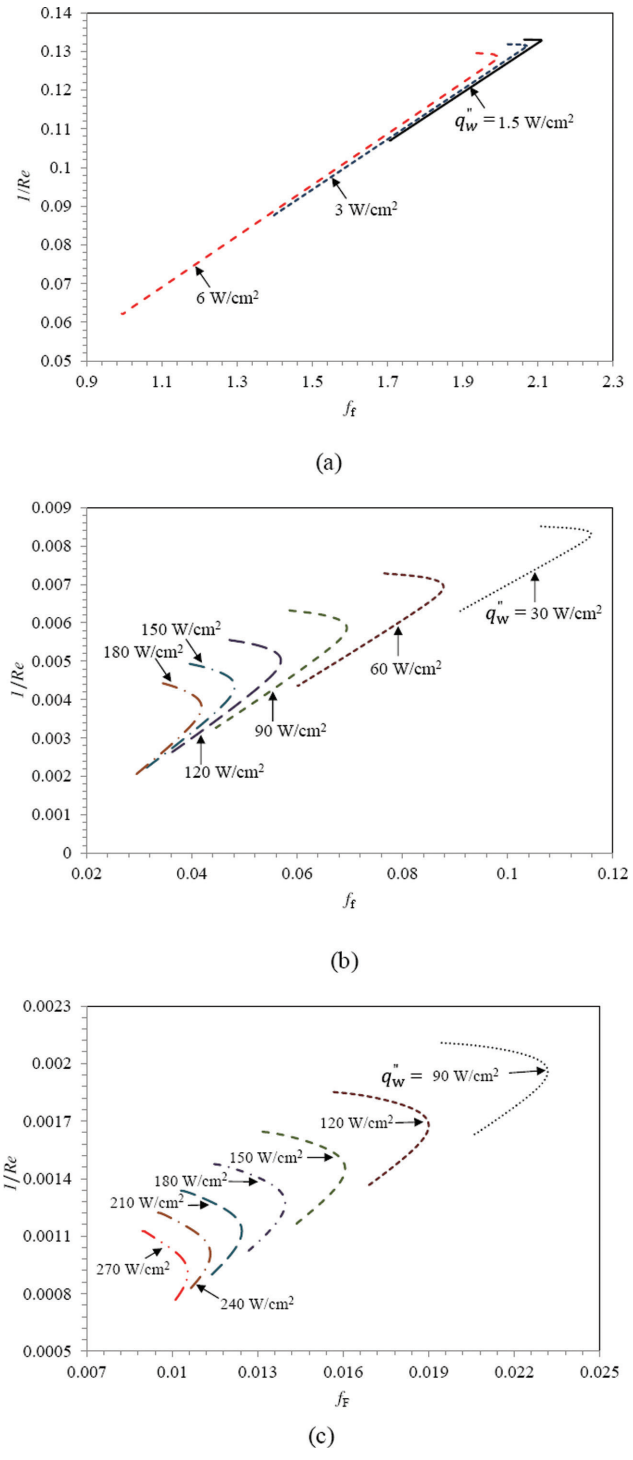

Figure 3. Variation of (1/*Re*) versus f_f: (a) $u_{m,in}$ = 0.075 m/s (Reynolds' analogy largely valid), (b) $u_{m,in}$ = 1 m/s, and (c) $u_{m,in}$ = 3 m/s (Reynolds' analogy largely invalid).

The role of $\Pi_{S\rho T}$, $\Pi_{S\mu T}$, and Π_{SkT} in flow friction is investigated considering combined $\rho(T)$, $\mu(T)$, and $k(T)$ variations. For large q''_w which is mainly allowed at high $u_{m,in}$, $\Pi_{S\rho T}$ emerged in continuity equation yields a strong effect on *Po*. Figure 6 gives the variation of *Po* versus $\Pi_{S\rho T}$, only Reynolds' analogy valid data has been taken for $u_{m,in}$ = 0.075, 1, and 3

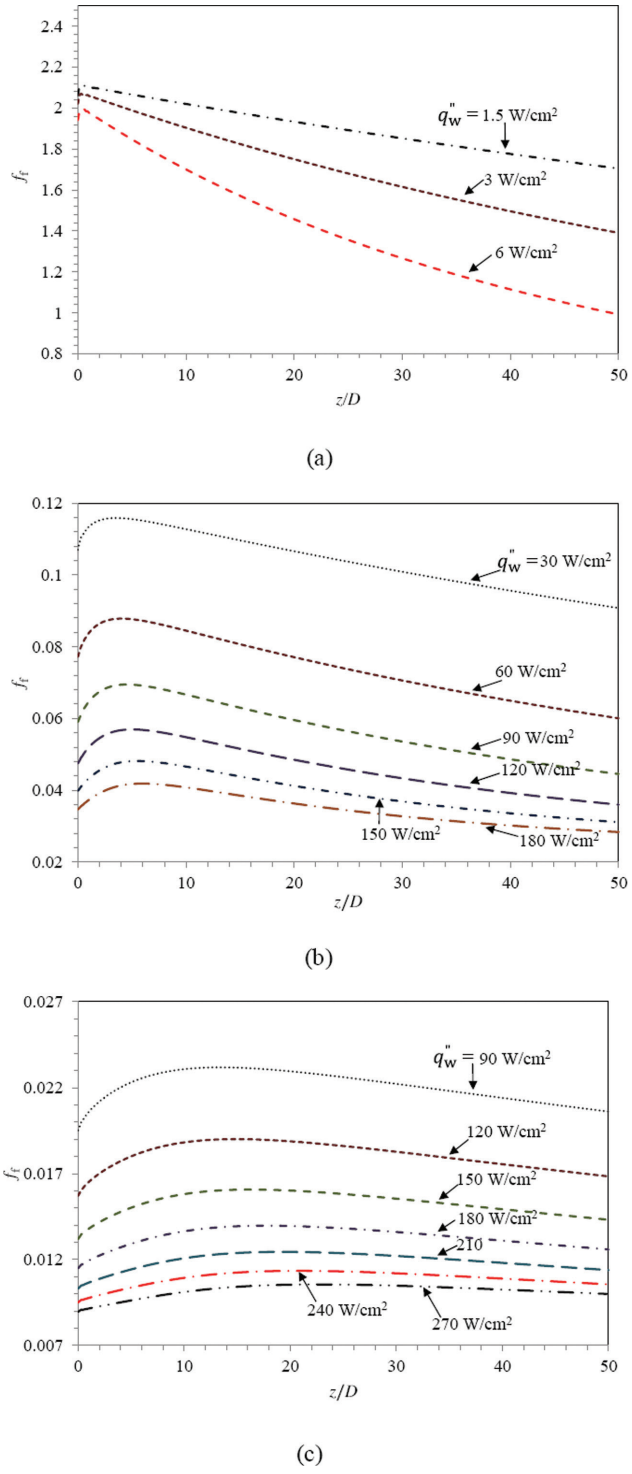

Figure 4. Variation in f_f along the flow: (a) $u_{m,in}$ = 0.075 m/s, (b) $u_{m,in}$ = 1 m/s, and (c) $u_{m,in}$ = 3 m/s.

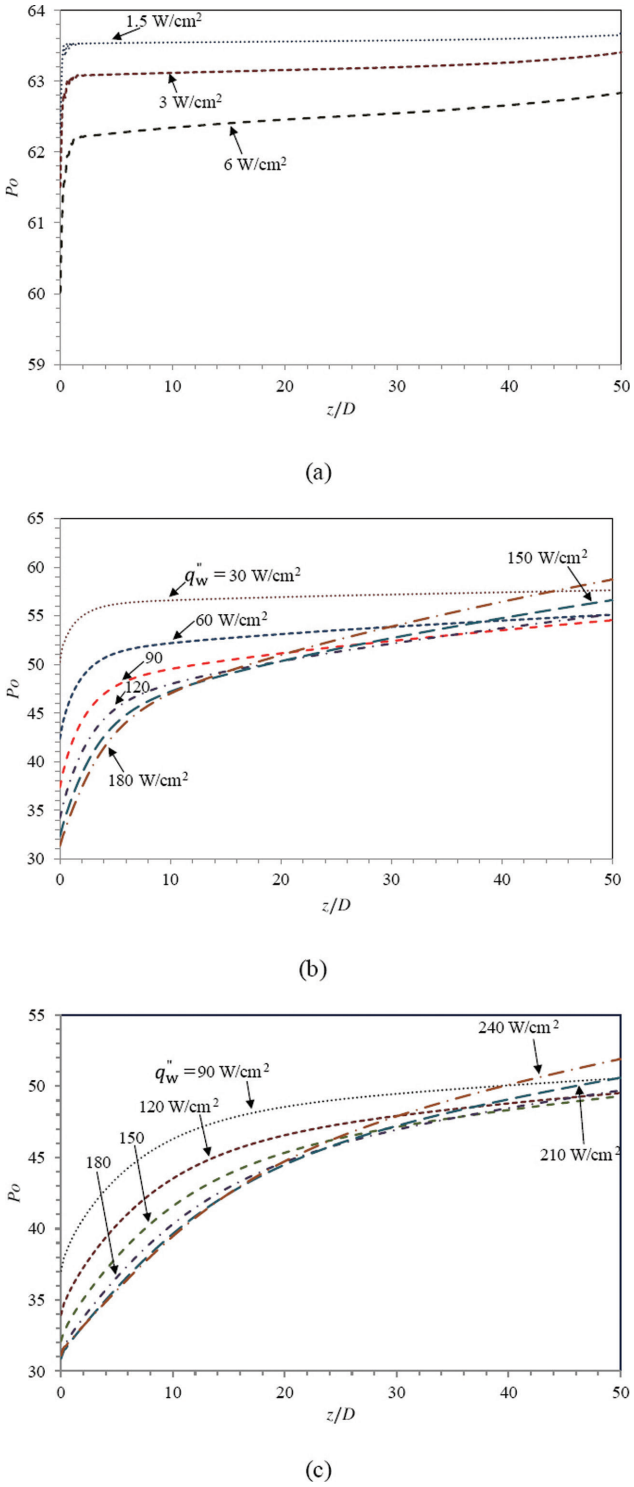

Figure 5. Variation in *Po* along the flow. (a) $u_{m,in}$ = 0.075 m/s, (b) $u_{m,in}$ = 1 m/s, and (c) $u_{m,in}$ = 3 m/s.

m/s. Figure 6 (a, b, c) illustrates that a similar pattern for different permissible is followed in the Reynolds analogy valid region. As increases, the value of $\Pi_{S\rho T}$ also increases, which indicates that the influence of ρ(*T*) variation increases on micro-convective flow. Therefore, in figure 6, the regression equations have been proposed to correlate *Po* with $\Pi_{S\rho T}$ at different $u_{m,in}$, in the Reynolds analogy valid region as given in Table 2.

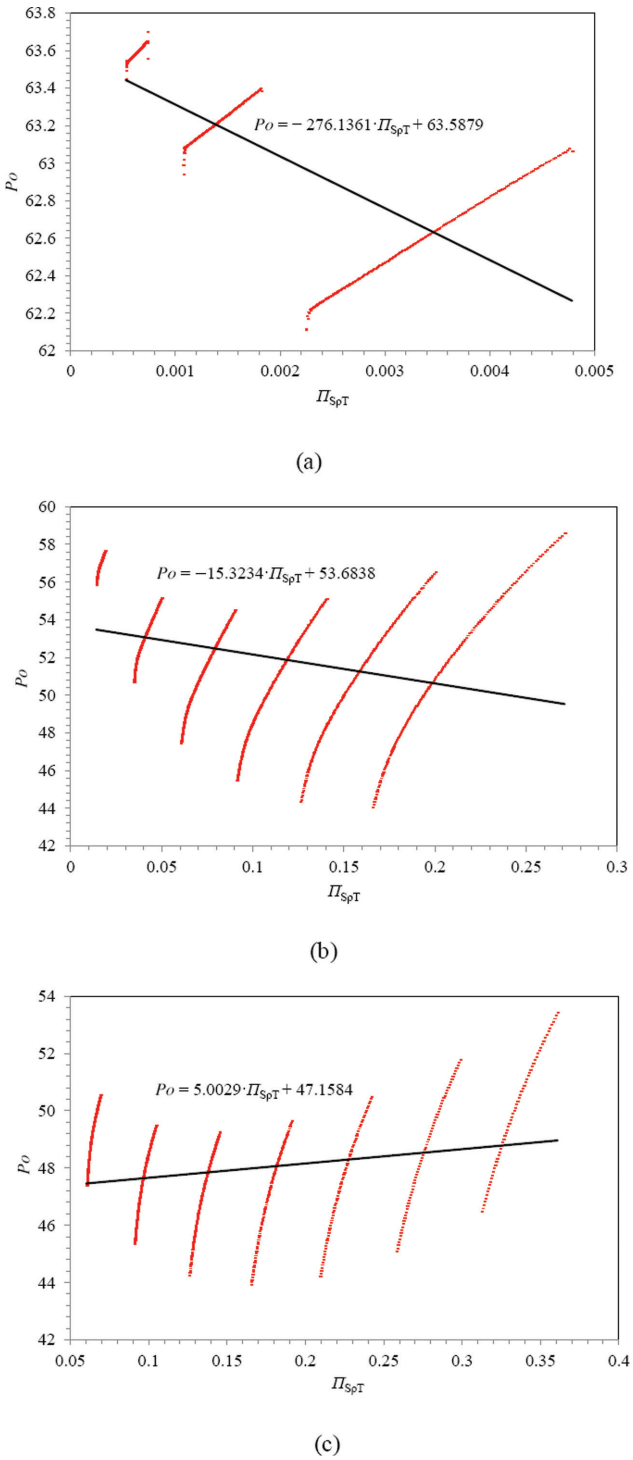

Figure 6. Variation of Po versus $\Pi_{S\rho T}$ (only Reynolds' analogy valid data): (a) $u_{m,in} = 0.075$ m/s, (b) $u_{m,in} = 1$ m/s, and (c) $u_{m,in} = 3$ m/s.

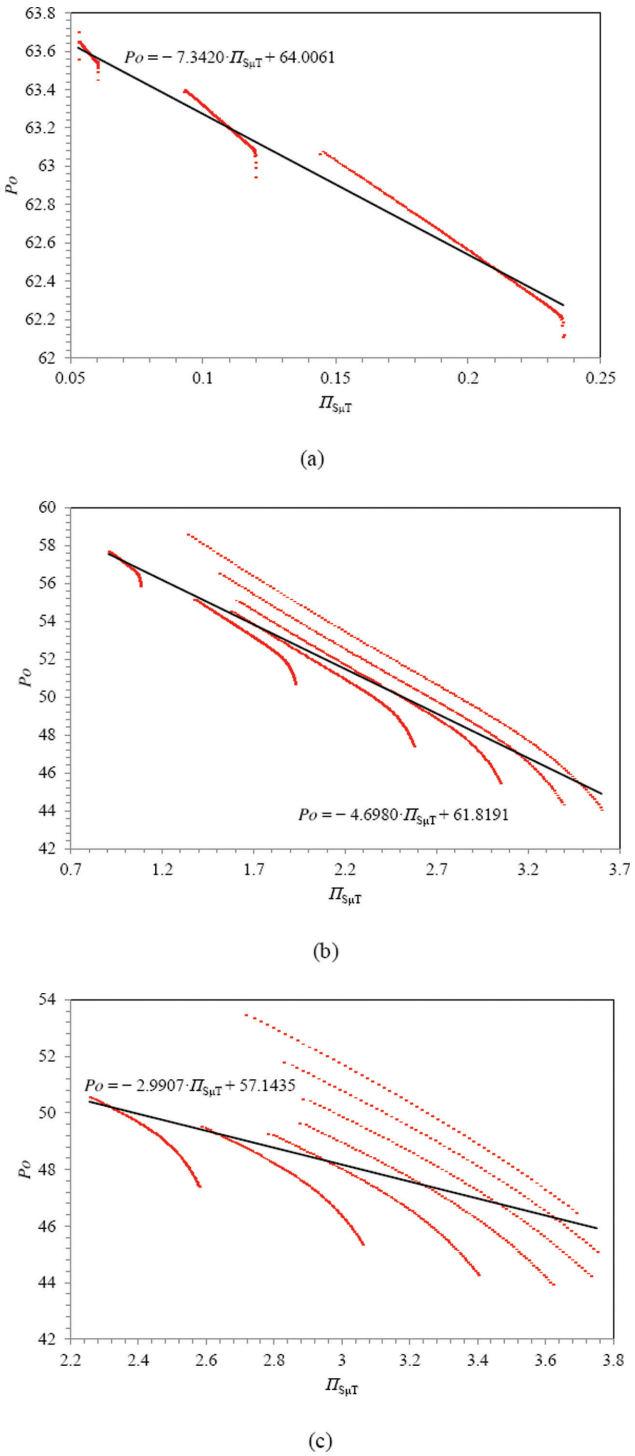

Figure 7. Variation of Po versus $\Pi_{S\mu T}$ (only Reynolds' analogy valid data). (a) $u_{m,in} = 0.075$ m/s, (b) $u_{m,in} = 1$ m/s, and (c) $u_{m,in} = 3$ m/s.

Figure 7 gives the variation of Po versus $\Pi_{S\mu T}$, only Reynolds analogy valid data has been taken for the same cases as in figure 6. Figure 7 (a, b, c) indicates a similar pattern for different allowable, in the Reynolds' analogy valid region. As q''_w increases, the value of $\Pi_{S\mu T}$ also increases, which shows the effect of $\mu(T)$ variation increases on micro-convective flow. Table 3 gives the regression equations which mathematically represent the correlation between

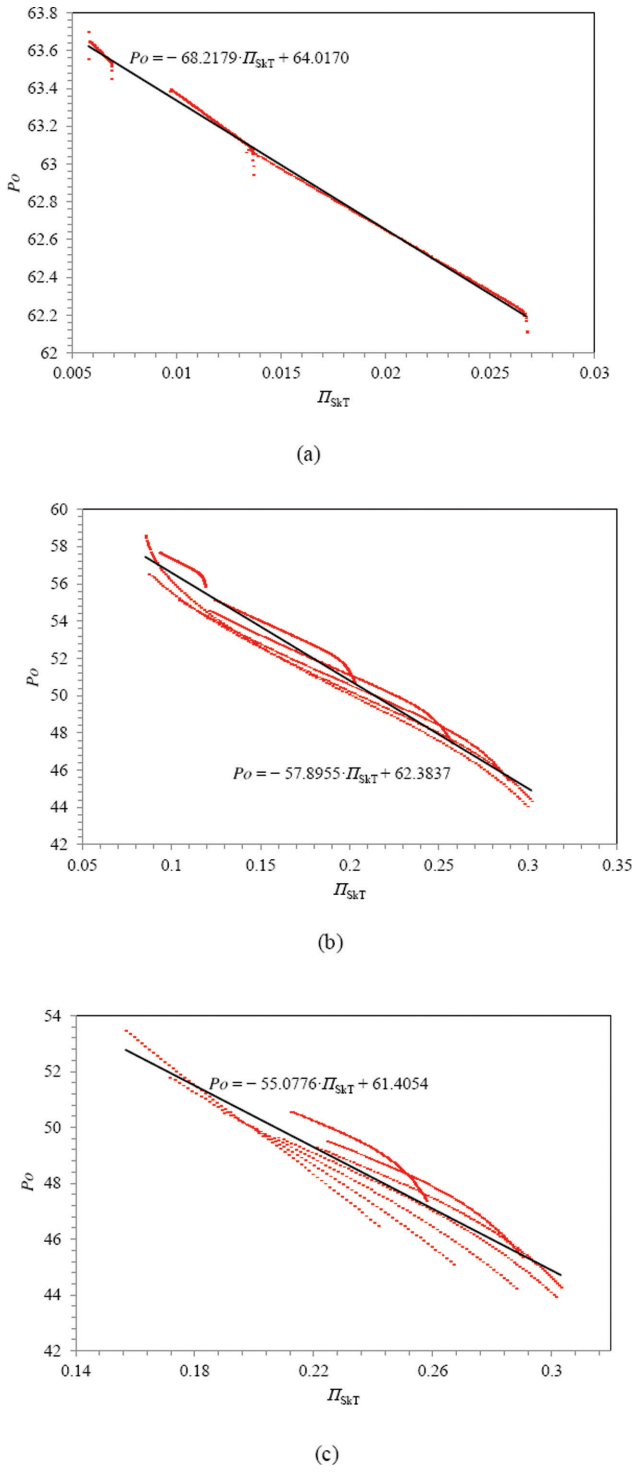

Figure 8. Variation of Po versus Π_{SkT} (only Reynolds' analogy valid data): (a) $u_{m,in}$ = 0.075 m/s, (b) $u_{m,in}$ = 1 m/s, and (c) $u_{m,in}$ = 3 m/s.

Po and $\Pi_{S\mu T}$, in the Reynolds analogy valid region at $u_{m,in}$ = 0.075, 1, and 3 m/s as shown in figure 7.

For large q''_w that is enabled at high $u_{m,in}$, Π_{SkT} also produces a strong effect on Po. Figure 8 illustrates the variation of Po versus Π_{SkT}, only Reynolds analogy valid data has been taken for the same cases as in figures 6, 7. From figure 8, it is observed that Π_{SkT} increases with an increase in q''_w, which shows the effect of $k(T)$ variation increases on micro-convective flow. Again a similar trend is observed for different allowable q''_w in the Reynolds analogy valid region as shown in figure 8 (a, b, c). Table 4 gives the estimated regression equations which mathematically represent the correlation between Po and Π_{SkT} for $u_{m,in}$ = 0.075, 1, and 3 m/s, in the Reynolds' analogy valid region as illustrated in figure 8.

The role of $\Pi_{S\rho T}$, $\Pi_{S\mu T}$, and Π_{SkT} in flow friction is expressed with the help of estimated regression equations. From these equations, it is observed that as $u_{m,in}$ increases, the effect of $\rho(T)$, $\mu(T)$, and $k(T)$ variations increases on micro-convective water flow.

Table 2. Estimated regression equations to correlate Po with $\Pi_{S\rho T}$

$u_{m,in}$ (m/s)	R^2	Estimated regression equations
0.075	0.5412	$Po = -276.1361 \cdot \Pi_{S\rho T} + 63.5879$
1	0.0905	$Po = -15.3234 \cdot \Pi_{S\rho T} + 53.6838$
3	0.0558	$Po = 5.0029 \cdot \Pi_{S\rho T} + 47.1584$

Table 3. Estimated regression equations to correlate Po with $\Pi_{S\mu T}$

$u_{m,in}$ (m/s)	R^2	Estimated regression equations
0.075	0.9897	$Po = -7.3420 \cdot \Pi_{S\mu T} + 64.0061$
1	0.9165	$Po = -4.6980 \cdot \Pi_{S\mu T} + 61.8191$
3	0.3732	$Po = -2.9907 \cdot \Pi_{S\mu T} + 57.1435$

Table 4. Estimated regression equations to correlate Po with Π_{SkT}

$u_{m,in}$ (m/s)	R^2	Estimated regression equations
0.075	0.9984	$Po = -68.2179 \cdot \Pi_{SkT} + 64.0170$
1	0.9608	$Po = -57.8855 \cdot \Pi_{SkT} + 62.3837$
3	0.8721	$Po = -55.0776 \cdot \Pi_{SkT} + 61.4054$

CONCLUDING REMARKS

1. The performance of the overall system is affected by HT rates. Therefore, significant efforts have been devoted to increase the HT rates and decrease the shear stress for improvement in the performance of the system. The Reynolds analogy is valid only for that portion of the flow regime, where St increases with decreasing f_f for TFP. Therefore, the Reynolds

analogy helps to find the flow regime in which HT increases while τ decreases for TFP.
2. The Reynolds analogy is largely valid at low mean velocities; however, the Reynolds analogy is largely invalid at high mean velocities.
3. Direct proportionality of $(1/Re)$ with f_f for a significant section of the flow regime, also validates the Reynolds analogy.
4. The significance of mass transport due to $\rho(T)$ variation is given in governing equation (3) and momentum transport in axial and radial directions due to $\mu(T)$ variation is given in governing equations (5, 7). The significance of energy transport by the axial fluid conduction due to $k(T)$ variation is given in the governing equation (9).
5. Higher values of the $\Pi_{S\rho T}$, $\Pi_{S\mu T}$, and Π_{SkT} parameters show a stronger effect on micro-convection due to TFP.
6. The regression equations have been proposed to correlate Po with $\Pi_{S\rho T}$, $\Pi_{S\mu T}$, and Π_{SkT}, in the Reynolds analogy valid region.

ACKNOWLEDGMENTS

The author is grateful to Prof. Shripad P. Mahulikar, Professor, Department of Aerospace Engineering, IIT Bombay, India, for giving valuable suggestions to improve the quality of the manuscript.

NOMENCLATURE

$c_p(T)$	Temperature-dependent specific heat at constant pressure [J·kg^{-1}·K^{-1}]
D	Diameter of micro-tube [m]
f	Darcy friction factor
f_f	Fanning friction factor
L	Length of micro-tube [m]
h	Heat transfer coefficient [W·m^{-2}·K^{-1}]
$k(T)$	Temperature-dependent thermal conductivity [W·m^{-1}·K^{-1}]
q''_w	Heat flux at the wall [W·m^{-2}]
$S_{\rho T}$	Density-temperature sensitivity $(\partial\rho/\partial T)$
S_{kT}	Thermal conductivity-temperature sensitivity $(\partial k/\partial T)$
$S_{\mu T}$	Viscosity-temperature sensitivity $(\partial\mu/\partial T)$
T_0	Inlet temperature [K]
T_m	Bulk mean temperature [K]
T_w	Wall temperature [K]
$u(r)$	Axial velocity profile in the radial direction [-]
$(\partial u/\partial r)_w$	Wall velocity gradient [s^{-1}]
Greek symbols	
ν	Kinematic viscosity [m^2·s^{-1}]
$\rho(T)$	Temperature-dependent density [kg·m^{-3}]
$c_p(T)$	Temperature-dependent specific heat at constant pressure [J·kg^{-1}·K^{-1}]
$k(T)$	Temperature-dependent thermal conductivity [W·m^{-1}·K^{-1}]
$\mu(T)$	Temperature-dependent viscosity [N·s·m^{-2}]
τ_w	Shear stress at the wall [N·m^{-2}]
S_{kT}	Thermal conductivity temperature sensitivity $(\partial k/\partial T)$
$S_{\mu T}$	Viscosity temperature sensitivity $(\partial\mu/\partial T)$
$S_{\rho T}$	Density temperature sensitivity $(\partial\rho/\partial T)$
Non-dimensional numbers	
Br_{qw}	Brinkman number based on wall heat flux [–]. $Br_{S\rho T}$; $Br_{S\mu T}$; Br_{SkT} Modified Brinkman numbers based on temperature sensitivities of ρ, μ, and k respectively.
Nu	Nusselt number $(h\cdot D/k_m)$
Pe	Peclet number $(\rho_m\cdot u_m\cdot c_p\cdot D/k_m)$
Po	Poiseuille number $(f\cdot Re_D)$
Pr	Prandtl numbers $(c_p\cdot\mu_m/k_m)$
Re	Reynolds number $(\rho_m\cdot u_m\cdot D/\mu_m)$
St	Stanton number $(h/(\rho\cdot u_m\cdot c_p))$
Subscripts	
CP	Constant properties
D	Based on diameter
ex	Value at outlet
in	Value at inlet
m	Mean value of properties calculated at bulk mean temperature, T_m
VP	Variable properties
w	Condition at wall

DATA AVAILABILITY STATEMENT

The authors confirm that the data that supports the findings of this study are available within the article. Raw data that support the finding of this study are available from the corresponding author, upon reasonable request.

CONFLICT OF INTEREST

The author declared no potential conflicts of interest with respect to the research, authorship, and/or publication of this article.

ETHICS

There are no ethical issues with the publication of this manuscript.

REFERENCES

[1] Sieder EN, Tate GE. Heat transfer and pressure drop of liquids in tubes. Ind Eng Chem 1936;28:1429–1435. [CrossRef]

[2] Herwig H. The effect of variable properties on momentum and heat transfer in a tube with constant heat flux across the wall. Int J Heat Mass Transf 1985;28:423–431. [CrossRef]

[3] Herwig H, Voigt M, Bauhaus FJ. The effect of variable properties on momentum and heat transfer in a tube with constant wall temperature. Int J Heat Mass Transf 1989;32:1907–1915. [CrossRef]

[4] Kakaç S, Shah RK, Aung W. Handbook of single-phase convective heat transfer. John Wiley & Sons, Inc., New York, 1987.

[5] Harms TM, Jog MA, Manglik RM. Effects of temperature-dependent viscosity variations and boundary conditions on fully developed laminar forced convection in a semicircular duct. J Heat Transfer 1998;120:600–605. [CrossRef]

[6] Liu D, Lee PS. Numerical investigation of fluid flow and heat transfer in microchannel heat sinks. ME 605: In Convection of Heat and Mass, ASME, West Lafayette, IN, 2003.

[7] Andrade CR, Zaparoli EL. Effects of temperature-dependent viscosity on fully developed laminar forced convection in a curved duct. Int Commun Heat Mass Transf 2001;28:211–220. [CrossRef]

[8] Mahulikar SP, Herwig H, Hausner O, Kock F. Laminar gas micro-flow convection characteristics due to steep density gradients. Europhys Lett 2004;68:811. [CrossRef]

[9] Mahulikar SP, Herwig H. Theoretical investigation of scaling effects from macro-to-microscale convection due to variations in incompressible fluid properties. Appl Phys Lett 2005;86:014105. [CrossRef]

[10] Mahulikar SP, Herwig H. Physical effects in laminar microconvection due to variations in incompressible fluid properties. Phys Fluids 2006;18:073601. [CrossRef]

[11] Mahulikar SP, Herwig H. Physical effects in pure continuum-based laminar micro-convection due to variation of gas properties. J Phys D Appl Phys 2006;39:4116. [CrossRef]

[12] Nonino C, Del Giudice S, Savino S. Temperature dependent viscosity effects on laminar forced convection in the entrance region of straight ducts. Int J Heat Mass Transf 2006;49:4469–4481. [CrossRef]

[13] Herwig H, Mahulikar SP. Variable property effects in single-phase incompressible flows through microchannels. Int J Therm Sci 2006;45:977–981. [CrossRef]

[14] Mahulikar SP, Herwig H, Hausner O. Study of gas microconvection for synthesis of rarefaction and nonrarefaction effects. J Microelectromech Syst 2007;16:1543–1556. [CrossRef]

[15] Mahulikar SP, Herwig H. Fluid friction in incompressible laminar convection: Reynolds' analogy revisited for variable fluid properties. Eur Phys J B 2008;62:77–86. [CrossRef]

[16] Liu JT, Peng XF, Wang BX. Variable-property effect on liquid flow and heat transfer in microchannels. J Chem Eng 2008;141:346–353. [CrossRef]

[17] Gulhane NP, Mahulikar SP. Numerical study of compressible convective heat transfer with variations in all fluid properties. Int J Therm Sci 2010;49:786–796. [CrossRef]

[18] Gulhane NP, Mahulikar SP. Numerical study of microconvective water-flow characteristics with variations in properties. Nanoscale Microscale Thermophys Eng 2011;15:28–47. [CrossRef]

[19] Gulhane NP, Mahulikar SP. Numerical investigation on laminar microconvective liquid flow with entrance effect and Graetz problem due to variation in thermal properties. Heat Transfer Eng 2012;33:748–761. [CrossRef]

[20] Harley JC, Huang Y, Bau HH, Zemel JN. Gas flow in micr-channels. J Fluid Mechanics 1995;284:257–274. [CrossRef]

[21] Kumar R, Mahulikar SP. Effect of temperature-dependent viscosity variation on fully developed laminar microconvective flow. Int J Therm Sci 2015;98:179–191. [CrossRef]

[22] Kumar R, Mahulikar SP. Frictional flow characteristics of microconvective flow for variable fluid properties. Fluid Dyn Res 2015;47:065501. [CrossRef]

[23] Kumar R, Mahulikar SP. Numerical re-examination of Chilton–Colburn analogy for variable thermophysical fluid properties. J Heat Transfer 2017;139:071701. [CrossRef]

[24] Kumar R, Mahulikar SP. Heat transfer characteristics of water flowing through micro-tube heat exchanger with variable fluid properties. J Therm Anal Calorim 2020;140:1919–1934. [CrossRef]

[25] Kumar R, Mahulikar SP. Variable fluid property effect on heat transfer and frictional flow characteristics of water flowing through microchannel. J Eng Thermophysics 2018;27:456–473. [CrossRef]

[26] Kumar K, Kumar R, Bharj RS. Circular microchannel heat sink optimization using entropy generation minimization method. J Non-Equilib Thermodyn 2020;45:333–342. [CrossRef]

[27] Chauhan PR, Kumar R, Bharj RS. Optimization of the circular microchannel heat sink under viscous heating effect using entropy generation minimization method. Therm Sci Eng Prog 2019;13:100365. [CrossRef]

[28] Chauhan PR, Kumar K, Kumar R, Rahimi-Gorji M, Bharj RS. Effect of thermophysical property variation on entropy generation towards micro-scale. J Non-Equilib Thermodyn 2020;45:1-7. [Epub ahead of print]. doi: 10.1515/jnet-2019-0033. [CrossRef]

[29] Kumar R, Mahulikar SP. Effect of density variation on rarefied and non-rarefied gaseous flows in developing region of microtubes. Iran J Sci Technol Trans Mech Eng 2021;45:415–425. [CrossRef]
[30] Kumar R. Physical effects of variable fluid properties on gaseous slip-flow through a micro-channel heat sink. J Therm Eng 2021;7:635–649. [CrossRef]
[31] Keepaiboon C, Dalkilic AS, Mahian O, Ahn HS, Wongwises S, Mondal PK, et al. Two-phase flow boiling in a microfluidic channel at high mass flux. Phys Fluids 2020;32:093309. [CrossRef]
[32] Gaikwad HS, Roy A, Mondal PK, Chimres N, Wongwises S. Irreversibility analysis in a slip aided electroosmotic flow through an asymmetrically heated microchannel: The effects of joule heating and the conjugate heat transfer. Anal Chim Acta 2019;1045:85–97. [CrossRef]
[33] Sarma R, Gaikwad H, Mondal PK. Effect of conjugate heat transfer on entropy generation in slip-driven microflow of power law fluids. Nanoscale Microscale Thermophys Eng 2017;21:26–44. [CrossRef]
[34] Sarma R, Jain M, Mondal PK. Towards the minimization of thermodynamic irreversibility in an electrically actuated microflow of a viscoelastic fluid under electrical double layer phenomenon. Phys Fluids 2017;29:103102. [CrossRef]
[35] Kumar R, Mahulikar SP. Physical effects of variable thermophysical fluid properties on flow and thermal development in micro-channel. Heat Transfer Eng 2018;39:374–390. [CrossRef]
[36] Geankoplis CJ. Transport Processes and Separation Process Principles:(includes unit operations). Prentice Hall Professional Technical Reference, 2003.
[37] Bird RB, Stewart WE, Lightfoot EN. Transport Phenomena, Wiley, New York, 2002.
[38] Holman JP. Heat Transfer, McGraw-Hill, New York, 1990.
[39] McCutcheon SC, Martin JL, Barnwell TO. Handbook of Hydrology, McGraw-Hill, New York, 1993.
[40] Sherman FS. Viscous Flow, McGraw-Hill, New York, 1990.